Wavelet Measurement Suggests Cause of Period Instability in Mammalian Circadian Neurons

Kirsten Meeker[1], Richard Harang[2], Alexis B. Webb[3], David K. Welsh[4], Francis J. Doyle III[5], Guillaume Bonnet[2], Erik D. Herzog[3], Linda R. Petzold[1]

[1]Department of Computer Science, University of California, Santa Barbara, CA

[2]Department of Statistics and Applied Probability, University of California, Santa Barbara, CA

[3]Department of Biology, Washington University, St. Louis, MO

[4]Department of Psychiatry, University of California, San Diego, La Jolla, CA

Center for Chronobiology, University of California, San Diego, La Jolla, CA

Veterans Affairs San Diego Healthcare System, San Diego, CA

[5]Department of Chemical Engineering, University of California, Santa Barbara, CA

Correspondence to: Linda R. Petzold,[1] Department of Computer Science, University of California, Santa Barbara, CA 93106-5110, USA, Tel.: +1 805 893 5362; Fax: +1 805 893 5435 Email: petzold@cs.ucsb.edu.

Abstract

Cells in the suprachiasmatic nucleus (SCN) display remarkable precision, while either physically or chemically decoupling these cells from each other leads to a dramatic increase in period-to-period variability. Where previous studies have classified cells as either arrhythmic or circadian, our wavelet analysis reveals that individual cells, when removed from network interactions, intermittently express circadian and/or longer infradian periods. We reproduce the characteristic period distribution of uncoupled SCN cells with a stochastic model of the uncoupled SCN cell near a bifurcation in Bmal1 transcription repression. This suggests that the uncoupled cells may be switching between two oscillatory mechanisms: the indirect negative feedback of protein complex PER-CRY on the expression of Per and Cry genes, and the negative feedback of CLOCK-BMAL1 on the expression of Bmal1 gene. The model is particularly sensitive near this bifurcation point, with only a small change in Bmal1 transcription repression needed to switch from the stable precision of coupled SCN cells to the unstable oscillations of decoupled individual cells, making this rate constant an ideal target for cell signaling in the SCN.

Keywords: Suprachiasmatic Nucleus; Wavelet analysis; Bifurcation analysis; Stochastic model; Synchronization; Entrainment

Introduction

Disorders of circadian timekeeping may be an underlying cause of diseases that have become more prevalent in modern times since the invention of the electric light (Moore-Ede et al., 1983). In mammals the suprachiasmatic nucleus (SCN), a brain region of about 20,000 neurons, serves as the master circadian clock (Welsh et al., 2010) coordinating timing throughout the body and entraining the body to daily light cycles. Experiments in which cell-to-cell signaling between SCN neurons is disrupted by physical separation of the cells (Herzog et al., 2004) or by blocking vasoactive intestinal polypeptide (VIP) mediated signaling (Aton et al., 2005) show that the remarkable precision of the circadian clock at the level of the organism relies on this intercellular signaling. In the absence of cell-to-cell signaling, each SCN neuron and the SCN as a whole have significantly less stable oscillations. This has been measured in PER2::LUC bioluminescence recordings, firing rate recordings, and animal behavioral data.

Quantification and identification of the potential cause of the period instability in individual cells is an important step toward understanding the SCN system. Previous studies evaluated the distribution of periods over time (see Aton et al. (2005); Herzog et al. (2004); Levine et al. (2002)) using Fourier-based methods. Wavelet decomposition is better suited for capturing the temporal period variability observed in individual cells, and has been used on a wide range of biological oscillators (Addison, 2005; Baggs et al.,

2009; Bartnik et al., 1992; Brai and Stefanovska, 1998; Klevecz and Murray, 2001; Kong et al., 1998; Morlet et al., 1991; Price et al., 2008). Stochastic models based on small 3-state and 5-state deterministic models have demonstrated that individual cells display an increase in period variability as either the number of molecules is reduced, or model parameters are adjusted to be near a bifurcation point where oscillations cease (Forger and Peskin, 2005; Gonze and Goldbeter, 2006).

We combine Morlet continuous wavelet transform (CWT) analysis as described by Mallat (1999) and Torrence and Compo (1998) with a detailed stochastic model of gene regulation in SCN neurons to investigate the cause of period instability in individual SCN neurons. We compare PER2::LUC bioluminescence of dispersed SCN wild-type neurons from two labs (Ko et al., 2010; Liu et al., 2007; Webb et al., 2009) to a stochastic model derived from the 16-state deterministic Leloup and Goldbeter gene regulatory network model (Leloup and Goldbeter, 2003, 2004). This reconstruction and the use of a more detailed model provide novel insight into potential biological mechanisms underlying the observed period variability in decoupled SCN neurons.

Materials and Methods

Experimental Procedure for Collecting Circadian SCN Data

Single cell data were previously published in Liu et al. (2007), Ko et al. (2010), and Webb et al. (2009), and were obtained according to methods described therein. Briefly, SCN neurons with or without various clock gene knockouts were dispersed from 1-7 day old PER2::LUC reporter mice (Yoo et al., 2004) and cultured for up to 5 weeks at a density of 100-300 cells/sq mm in medium containing 5-10% fetal bovine serum. For comparison to dispersed cultures, neurons were also cultured with relatively intact tissue organization as SCN slices. For imaging, cells were transferred to serum-free, HEPES-buffered medium containing B27 supplement and luciferin, placed on the stage of an inverted microscope kept at 36-37 °C, and imaged with a low-noise CCD camera. Circadian clock function was measured as a time series of PER2::LUC bioluminescence intensities for single cells in 30-60 minute intervals over 6-8 days. For additional details on bioluminescence imaging methods, see Welsh et al. (2005, 2010). All animal procedures were approved and performed in accordance with local institutional guidelines as indicated in Webb et al. (2009), Liu et al. (2007), and Ko et al. (2010).

These data were collected in two different labs. Although methods used to collect these data were broadly similar, a number of differences could have affected the results. For example, Webb et al. used mice of a pure C57/BL6

genetic background instead of a mixed background, lower cell density of 100 cells/sq mm instead of 300 cells/sq mm, and started imaging sooner at 4 days in culture instead of 2-7 weeks in culture. Accordingly, the wild type datasets from the two different labs were analyzed separately (Liu et al., 2007; Webb et al., 2009).

Wavelet Tools for Analysis of Circadian Data

Well-established Fourier-based methods used to classify and analyze bioluminescence data in circadian oscillators share the common implicit assumption that the data are strongly stationary, and have a fixed frequency for the duration of the data (Levine et al., 2002). Such methods can misclassify nonstationary signals as either having a single period (see, for example, Figure 9 in the Supplement) or as being aperiodic due to the spread of signal intensity over a range of frequencies (Mallat, 1999). This may reduce the statistical significance of any individual frequency below the limits of detection. Thus, for the analysis of the nonstationary data presented in this paper, we selected the Morlet wavelet, which is closely related to the familiar tools of Fourier analysis (Bartnik et al., 1992; Mallat, 1999), and can be considered as a technique to adaptively window a Fourier transform in such a way that the temporal duration of the window is adjusted to each frequency being analyzed. The direct application of the Morlet wavelet allows for simultaneous estimation of phase, frequency, and amplitude of a particular data set while simultaneously detrending it, all without the strong parametric assumptions

that cause difficulty for traditional methods (Baggs et al., 2009).

Wavelets, including the Morlet wavelet, have been successfully used to analyze biological data across a wide range of time scales such as ECG signals (Addison, 2005; Kong et al., 1998; Morlet et al., 1991), EEG signals (Bartnik et al., 1992), human blood-flow dynamics (Brai and Stefanovska, 1998), and yeast RNA transcription data (Klevecz and Murray, 2001). The Morlet wavelet has also seen use in analysis of circadian period shifts and multiple simultaneous oscillations due to gene knockout/knockdown in mice (Price et al., 2008), as well as use in constructing gene association networks for oscillators of the mammalian circadian clock (Baggs et al., 2009).

Price et al. (2008) focuses on the use of the CWT in analyzing individual time series for the presence or absence of infradian and ultradian rhythms, and Baggs et al. (2009) apply the time-frequency decomposition properties of the CWT to determine gene network structure in the SCN. We extend these results by considering the distributional properties of the circadian period as measured by PER2::LUC photon emissions. We focus on pooling data from the CWT analysis of multiple circadian oscillators in order to evaluate properties of the overall period distribution.

Briefly, applying the Morlet wavelet to a data series generates a Continuous Wavelet Transform table: a complex-valued field across scales (corresponding to frequencies), and translations (corresponding to time). This set of complex values is often converted to radial coordinates and each coordinate magnitude and phase angle is plotted separately as a function of scale

and translation. Here we consider only the magnitude plots (see, for example, the lower panes of Figure 1). The magnitude of the complex value at any scale and translation indicates the approximate strength of the frequency corresponding to the selected scale at a time corresponding to the translation (Mallat, 1999). The final row of the table – the "scaling coefficients" – provides information about all low-frequency components of the signal beyond the resolution of the CWT table, including shifting baselines and the mean power of the signal.

By selecting a series of points across translations at which the magnitude of the CWT reaches local maxima (the "CWT ridges"), estimates of the frequency evolution of the periodic components of the signal can be obtained. The scales of the CWT ridge are typically converted back to frequency or period (see e.g. Torrence and Compo (1998)) while the translations are used to indicate time. Once recovered from the CWT heat map, the CWT ridge may be considered as a list of wavelength-translation pairs, where each point represents the strongest oscillatory component of the cell at that time point. In some cases, particularly when noise levels are high and multiple oscillators may be contributing to the signal, simply selecting the global or local maxima at each translation may not be the optimal method of extracting the CWT ridge (see Abid et al. (2007) for an overview of ridge extraction techniques and their associated issues, and Carmona et al. (1999) for the "Crazy climber" algorithm used in Baggs et al. (2009)). Tracking the period of the oscillator by selecting the translation-by-translation maximum (Carmona et al., 1997)

from the CWT table provides a robust, rapid, and deterministic method for generating the ridge plot and examining the frequency evolution of the oscillator over time, allowing us to characterize the variation in dominant period of the cell and consider the source of this variability.

The initial CWT analysis that all of the following analyses and period distribution estimates are based on was performed as follows: to reduce edge effects, the original data for analysis were first mean-centered and then padded with an equal length of zeros at the beginning and end of the data set. The CWT was calculated in the Fourier domain using methods described in Mallat (1999) and Torrence and Compo (1998). The standard representation of scales as voices within octaves (see Mallat (1999) and Torrence and Compo (1998) for details) was used, with 64 voices per octave, which was found to provide adequate resolution. Note that the range of periods that can be measured in a data set is limited by the sample rate and the length of the experiment. Following the computation of the inverse Fourier transform, the resulting CWT table was truncated to the length of the original data series in order to remove the zero-padding. The translation-by-translation maximum of the norm was selected as the ridge, and the scale at which that maximum occurred was extracted and converted back to instantaneous period as described in Mallat (1999) and Torrence and Compo (1998). Ridges were identified via translation-by-translation maxima as described above. Ridges that fell into the scaling coefficients of the CWT were identified with loss of periodicity and no dominant period was recorded for those time points;

the scaling coefficients are also excluded from the histograms and heatmaps presented throughout.

Computational Model

A deterministic model of the mammalian circadian gene network, developed by Leloup and Goldbeter (Leloup and Goldbeter, 2003, 2004), was chosen for conversion to a stochastic model because it contained enough detail to trace period instabilities to the underlying biological mechanisms and provided Per mRNA levels for comparison with PER2:LUC biological experiment data. The use of a stochastic model allowed us to examine whether period fluctuations due to molecular reaction events could be the cause of PER protein period instability in SCN neurons.

We converted the deterministic model into a stochastic model by changing reaction rates to propensities for discrete reaction events, and converting concentrations of chemical species to population counts (see Supplement). Time-dependent solutions were computed using the Stochastic Simulation Algorithm (SSA) due to Gillespie (1976) and implemented in the C programming language. Initial conditions were selected randomly from a previous simulation, which was run long enough for any transients to settle. This randomization of initial conditions along with the random firing of reactions during the simulation gave each simulated cell a unique time history.

Following the procedure for continuation analysis of an oscillatory system XPPAUTO (Ermentrout, 2001) was utilized to compute the period as

a function of model parameters (Figure 4). The identical wavelet analysis (implemented in MATLAB) to that used on the biological data was used to analyze the model data.

Results

Wavelet Analysis Reveals Non-Stationary Periods

We use CWT analysis as described above to recover period information from the SCN oscillators. Figure 1 displays examples of the initial CWT analysis performed on three individual cells; the traces in the upper panels correspond to the heatmaps in yellow, white, and red in the lower panels, which are used to generate the ridges highlighted in green. Each ridge point indicates the dominant oscillatory period for the cell at the indicated time; this analysis is repeated across all cells in the data set (see Supplement for more examples).

For oscillators that exhibit strongly stochastic behavior, distributional information about the period of the oscillator is much more relevant than examining the time-frequency evolution of a single realization – as proposed in Price et al. (2008) and used in Baggs et al. (2009). We utilize both period variability histograms and period distribution plots to examine this distributional behavior of SCN oscillators.

Period variability histograms (Figure 2) display the period variability of various populations of SCN cells as inferred by CWT analysis; each cell's instantaneous period over time was estimated individually using the CWT

as described above, and the standard deviation of that period over time was calculated to estimate the stability of the cell's oscillations. The results using CWT analysis are consistent with those described in Herzog et al. (2004) and Aton et al. (2005): dispersed SCN cells display a significantly broader range of period standard deviations than coupled SCN cells. Note that the slice data from both labs (Figure 2, A and C) displays a significantly tighter cluster of variances than the corresponding dispersed data, but that the modal variance is not zero, indicating that there is some inherent variability in the periods of even coupled SCN cells. Analysis of cells decoupled by physical dispersion (Figure 2, B and D) illustrate that the range of period variability increases significantly in the absence of intracellular communication.

The distribution of instantaneous periods across time for a pooled population of SCN oscillators is displayed in period distribution plots. A simple histogram of instantaneous periods is created for each cell (see Supplement, Figure 5, blue lines, for individual cell examples), and a population histogram is assembled to visualize the period distribution over a population of cells. Figure 3 (A and B) compares the period distribution of coupled and dispersed cells. As expected from previously published results, the dispersed cell period distribution is wider than that of coupled cells in an SCN slice. Dispersed cells spend half of their time at periods between 23-42 hrs. (data from Webb et al. (2009)) or 22-30 hrs. (data from Liu et al. (2007)), while coupled cells spend half of their time at a narrower range of periods between 24-29 hrs. The period distribution of dispersed cells also has a long period

tail up to 48-53 hours, while at the same time there are few periods shorter than 18 hours. The long period tail observed here by using wavelet analysis is a distinguishing characteristic of the underlying stochastic processes driving the oscillations.

While cellular heterogeneity is one possible explanation for the overall population distribution of periods, both direct examination of individual cell plots (see Figure 1 and Supplemental Figures 1 and 2) as well as analysis of the frequency distribution of individual cells reveal that an assumption of heterogeneity does not appear to be required to explain these data. Most dispersed wild-type SCN cells have circadian periods (20-30 hrs.) most of the time. Across all cells 79.4% of all recorded oscillations are in the circadian range. However, the majority of cells (67.6%, 255 out of 377) also exhibit non-circadian behavior, a dominant period outside of 20-30 hrs. There are only a few cells (5.8%, 22 out of 377) that have no dominant period within the circadian range. We therefore conclude that a heterogeneous population of cells oscillating with different periods is not needed to reproduce the distribution of periods observed in biological cells (Figure 3). The observed period distribution across the cell population may be obtained from a homogeneous population of cells where each cell is a stochastic oscillator with a non-stationary period; such a population will necessarily include cells that – due to the stochastic nature of their oscillations – do not exhibit any circadian behavior during the short time for which they are observed. Detailed visualization of individual cells in the Supplement (see Supplemental Fig-

ures 1 and 2) illustrate the varied behaviors cells can display within a single brief time series, supporting the conclusion that a homogeneous population of stochastic oscillators is adequate to explain the observed data.

To control for the possibility that the observed long periods are artifacts, we follow a Monte Carlo procedure as described in detail in the Supplement. Briefly, null distributions for period distribution are generated from both $1/f$-type noise – a stochastic process with significant serial correlations – and bioluminescence data generated by BMAL1 knockout cells. We consider BMAL1 knockout cells a good representation of arrhythmic cells because they do not display any dominant oscillation period. Distributional estimates for the period histograms are formed by modeling the data as the output of a multinomial distribution and obtaining the distribution of the underlying probability vector using conjugate priors. Random samples from these null distributions are then taken and compared to random samples taken from posterior distributions generated using the biological data, investigating infradian periods of 36 hours or longer. Comparing a large number of pairwise samples drawn in such a manner allows us to estimate p-values of the observed data against the two null hypotheses. Dispersed cells from both labs have statistically significant infradian periodicities at a p-value of $p < 0.01$ (see Supplement, Figure 6). Complete details and results are available in the Supplement.

As Poisson noise has spectral characteristics which change slightly with the mean of the signal, a different approach is taken to test for statistical

significance against a null hypothesis of Poisson noise. Rather than testing the population, each cell is tested individually against a homogeneous Poisson process with a mean equal to the original signal. Statistical significance for each individual cell at each individual period is then evaluated at a p-value of < 0.01, and the proportion of cells that contain statistically significant power at each period band are then tallied. Dispersed data from both Liu et al. (2007) and Webb et al. (2009) indicate that a number of individual cells display statistically significant power at a range of infradian periods (Supplement Figures 3 and 4). As above, complete details are accessible in the Supplement.

Modeling Provides a Possible Mechanism

An increase in period variability can be achieved either by reducing the number of molecules in the stochastic model, or by adjusting model parameters to be near a bifurcation point where oscillations are less stable. In this study we consider both techniques and show results from the following model variants: a discrete stochastic version of the Leloup and Goldbeter model (Leloup and Goldbeter, 2003) as the number of molecules is reduced; near a non-oscillatory bifurcation point of the mean *Period* gene (*Per*) transcription rate ν_{sP}; near an unstable range in the *Bmal1* gene transcription repression K_{IB}; and near an unstable range in the mean *Bmal1* gene transcription rate ν_{mB} (Figure 4).

Surprisingly, by lowering the molecular count alone, we are not able to

reproduce the biological period distribution. As the molecular population is lowered the period distribution does widen (Figure 3-C), but does not exhibit the long-periods observed in the biological data. Next we test the model near a non-oscillatory bifurcation point of mean *Per* transcription rate ν_{sP}. This model variation was used in To et al. (2007) to produce a heterogeneous population of cells with a desired percentage of oscillatory and non-oscillatory cells. It has the advantage that increasing *Per* transcription through inter-cellular coupling restores rhythmicity to all the cells, which is a necessary condition for inter-cellular synchrony. Approaching the ν_{SP} bifurcation widens the period distribution (Figure 3-D); however the long periods which we have shown to be significant in our analysis in the previous section are not reproduced.

To determine how the stochastic model can be made to produce the long periods, bifurcation analysis of the deterministic Leloup and Goldbeter model is employed. Our analysis identifies two sets of parameters that are capable of producing the longer periods observed in the dispersed cell data. The first set (Figure 4 left column) is associated with the PER-CRY feedback loop and requires an order of magnitude change in value to produce the period range. The second set (Figure 4 right column) is associated with the CLOCK-BMAL1 feedback loop or global scale factors, and produces the observed period range with less than an order of magnitude change. Global parameters ν_{sTot} and k_{sTot} change the transcription and protein production rates of all three key genes. Changes in these global parameters are reflected

in the *Bmal1* mRNA transcription rate and BMAL1 protein production rate, and so produce the same 2 branch bifurcation behavior found in parameters affecting the production of *Bmal1* mRNA.

For the second set of parameters, the period versus parameter functions all have two oscillatory branches connected by an unstable oscillatory segment. Leloup and Goldbeter (Leloup and Goldbeter, 2004) identified each of the two oscillatory branches with one of the feedback loops present in the circadian clock. Song et al. (2007) demonstrated that a simple model consisting of interlocked positive and negative feedback loops could behave as either a bistable switch or an oscillator depending on the relative strengths of the two feedback loops. Selecting parameter values that allow switching between the oscillatory branches provides a mechanism by which longer periods may be generated by the model.

The *Bmal1* transcription repression K_{IB} and transcription rate ν_{mB} are chosen from the second group of parameters for their maximum period value and sensitivity. Stochastic simulation results (Figure 3-E) show that as K_{IB} is increased the period distribution of the stochastic model widens, creating a longer tail on the distribution of infradian periods, and at the same time increasing the mean period.

To quantify the difference between period distributions, the Kullback-Leibler (KL) divergence (Kullback and Leibler, 1951) is used. The Kullback-Leibler divergence provides a measure of "distance" or "divergence" between statistical densities in terms of relative information gain. Smaller values of

the KL divergence indicate two distributions that are more nearly similar. Increasing the *Bmal1* transcription repression K_{IB} produces the lowest KL divergence (Table 1) while preserving oscillatory behavior and hence produced the best period distribution fit among the models studied (Figure 3).

Discussion

We show that individual SCN cells, when uncoupled from network interactions, are capable of producing a wide range of periodic behaviors which vary over time. Analysis of the period distributions show that the majority of cells (over 80%) are capable of producing at least transient circadian rhythms over the length of the observed data. This result agrees with previous studies (Liu et al., 2007; Webb et al., 2009; Welsh et al., 1995) which report that 53% to 80% of dispersed SCN cells express circadian rhythms. However, our wavelet visualization also reveals that nearly 10% of all dispersed cells have statistically significant ($p < 0.01$) instantaneous periods ranging from 40 to 46 hours.

Though it is possible that the long periods could be due to multiple oscillators, such as those found in dinoflagellates (Roenneberg and Morse, 1993), we assume that is not the case and measure the single strongest period at each instant of time. Visualization of the periodic behavior of the individual cells over time via CWT ridge plots shows that this variation in periodic behavior occurs within individual cells. This suggests that SCN cells are noisy oscillators that are homogeneous in their ability to produce transient

circadian rhythms.

We reproduce the period distribution observed in dispersed cells with the stochastic model by operating near a bifurcation point in the *Bmal1* transcription repression parameter. Leloup and Goldbeter (Leloup and Goldbeter, 2004) identified each of the two oscillatory branches in the *Bmal1* transcription repression parameter with two feedback loops in the circadian gene regulatory network. Selecting parameter values that allow switching between the oscillatory branches provides a mechanism for producing the observed period distribution. This requires only a modest change in parameter values. By comparing the behavior of the model at two different types of bifurcation points we illustrate that the distribution of the infradian periods is different between these two points, and that the wavelet analysis can distinguish these models and with the aid of the Kullback-Leibler divergence select the most appropriate model.

A central question regarding the SCN system is how does it produce such precise oscillations with so much period variability in individual cell oscillators? So far, in order to reproduce the individual cell period variability most models have required that they be operated near a bifurcation point (even at low molecular count). This investigation has pointed to a different type of bifurcation (between two oscillatory regimes) for reproducing dispersed cell period distributions than the fixed point bifurcations used in To et al. (2007) and Liu et al. (2007). The advantage of this type of bifurcation may be that by switching to a longer period without quenching oscillations the system

may be more easily shifted to a new light entrainment schedule.

The period distribution of the cell model is an important property for modeling synchronization in a system of coupled oscillators because it has an effect on the formation of clusters of synchronized cells (Kogan et al., 2008). Many questions remain to be answered about the coupled system. What intercellular mechanisms provide the stability observed in the coupled system? How does stochastic noise of individual cells contribute to stability and synchronization in the coupled SCN? It may be that the coupled system achieves greater stability through increased signal-to-noise provided by intercellular connectivity, while the presence of stochastic noise adds tractability to the SCN allowing it to more readily entrain to changes in light schedule.

Period variations imply that the phase response is also affected (Daan and Pittendrigh, 1976; Gonze and Goldbeter, 2006), so these findings may also be significant for modeling perturbation effects on the coupled system such as light entrainment. In addition to measuring the period, wavelets can be used to extract phase information. Our future work will focus on developing a coupled cell model using wavelet analysis to examine the phase of individual cells as they synchronize and respond to perturbations.

Acknowledgments

The authors wish to acknowledge the generous support of the agencies and grants that have funded this work: ICB grant through the Army Research

Office grant DAAD19-03-D-0004 (FJD); NIH grants GM078993, EB007511, and MH63109 (LRP); DOE grant DE-FG02-04ER25621 (LRP); the Army Research Office grant W911NF-07-1-0279 (FJD); NIH grant R01 MH082945 (DKW); and the VA Career Development Award (DKW).

Author contributions: KM did the model conversion, bifurcation analysis, and distributional analysis of the model and mutant data. RH wrote the analysis software and did the initial analysis of the biological data under supervision of GB as well as the statistical testing. DKW and ABW performed the biological experiments. KM and RH wrote the paper with contributions from all other authors. LRP, EDH, FJD, and DKW reviewed the manuscript and assisted with data analysis.

Conflict of interest statement: The authors declare that they have no conflict of interest.

References

A. Z. Abid, M. A. Gdeisat, D. R. Burton, and M. J. Lalor. Ridge extraction algorithms for one-dimensional continuous wavelet transform: a comparison. *Journal of Physics: Conference Series*, 76:012045, 2007. ISSN 1742-6596. URL http://www.iop.org/EJ/abstract/1742-6596/76/1/012045.

Paul S. Addison. Wavelet transforms and the ECG: a review. *Physiological Measurement*, 26(5):R155–R199, 2005. ISSN 0967-3334. URL http://www.iop.org.proxy.library.ucsb.edu:2048/EJ/abstract/0967-3334/26/5/R01.

Sara J Aton, Christopher S Colwell, Anthony J Harmar, James Waschek, and Erik D Herzog. Vasoactive intestinal polypeptide mediates circadian rhythmicity and synchrony in mammalian clock neurons. *Nat Neurosci*, 8 (4):476–483, April 2005. ISSN 1097-6256. URL http://dx.doi.org/10.1038/nn1419.

Julie E Baggs, Tom S Price, Luciano DiTacchio, Satchidananda Panda, Garret A FitzGerald, and John B Hogenesch. Network features of the mammalian circadian clock. *PLoS Biol*, 7(3):e1000052, March 2009. doi: 10.1371/journal.pbio.1000052. URL http://dx.doi.org/10.1371/journal.pbio.1000052.

E. Bartnik, K. Blinowska, and P. Durka. Single evoked potential reconstruc-

tion by means of wavelet transform. *Biological Cybernetics*, 67(2):175–181, June 1992. doi: {10.1007/BF00201024}. URL http://dx.doi.org/10.1007/BF00201024.

Maja Brai and Aneta Stefanovska. Wavelet-based analysis of human blood-flow dynamics. *Bulletin of Mathematical Biology*, 60(5):919–935, 1998. doi: 10.1006/bulm.1998.0047. URL http://dx.doi.org/10.1006/bulm.1998.0047.

R.A. Carmona, W.L. Hwang, and B. Torresani. Characterization of signals by the ridges of their wavelet transforms. *IEEE Transactions on Signal Processing*, 45(10):2586–2590, 1997. ISSN 1053-587X. doi: 10.1109/78.640725.

R.A. Carmona, W.L. Hwang, and B. Torresani. Multiridge detection and time-frequency reconstruction. *IEEE Transactions on Signal Processing*, 47:480–492, 1999. ISSN 1053-587X. doi: 10.1109/78.740131.

Serge Daan and Colin S. Pittendrigh. A functional analysis of circadian pacemakers in nocturnal rodents. *Journal of Comparative Physiology A: Neuroethology, Sensory, Neural, and Behavioral Physiology*, 106(3):253–266, October 1976. URL http://dx.doi.org/10.1007/BF01417857.

Bard Ermentrout. XPPAUT5.0—The differential equations tool. University of Pittsburgh, Pittsburgh. (http://www.pitt.edu/ phase/), 2001.

Daniel B. Forger and Charles S. Peskin. Stochastic simulation of the mammalian circadian clock. *Proceedings of the National Academy of Sciences of the United States of America*, 102(2):321–324, 2005. URL `http://www.pnas.org/content/102/2/321.abstract`.

Daniel T. Gillespie. A general method for numerically simulating the stochastic time evolution of coupled chemical reactions. *Journal of Computational Physics*, 22:403, 1976.

D. Gonze and A. Goldbeter. Circadian rhythms and molecular noise. *Chaos*, 16(2), June 2006.

Erik D. Herzog, Sara J. Aton, Rika Numano, Yoshiyuki Sakaki, and Hajime Tei. Temporal precision in the mammalian circadian system: A reliable clock from less reliable neurons. *Journal of Biological Rhythms*, 19:35–46, 2004.

Robert R. Klevecz and Douglas B. Murray. Genome wide oscillations in expression wavelet analysis of time series data from yeast expression arrays uncovers the dynamic architecture of phenotype. *Molecular Biology Reports*, 28(2):73–82, June 2001. doi: {10.1023/A:1017909012215}. URL `http://dx.doi.org/10.1023/A:1017909012215`.

Caroline H. Ko, Yujiro R. Yamada, David K. Welsh, Ethan D. Buhr, Andrew C. Liu, Eric E. Zhang, Martin R. Ralph, Steve A. Kay, Daniel B. Forger, and Joseph S. Takahashi. Emergence of Noise-Induced oscillations

in the central circadian pacemaker. *PLoS Biol*, 8(10):e1000513, October 2010. doi: 10.1371/journal.pbio.1000513. URL http://dx.doi.org/10.1371/journal.pbio.1000513.

Oleg Kogan, Jeffrey L. Rogers, M. C. Cross, and G. Refael. Renormalization group approach to oscillator synchronization. *Physical Review E*, 2008. URL http://arxiv.org/abs/0810.3075.

Jun Kong, Zheru Chi, and Weixue Lu. Electrocardiogram compression using modulus maxima of wavelet transform. In *Proceedings of the 20th Annual International Conference of the IEEE, Engineering in Medicine and Biology Society, 1998.*, volume 3, pages 1527–1530 vol.3, 1998. doi: {10.1109/IEMBS.1998.747178}.

S. Kullback and R. A. Leibler. On information and sufficiency. *The Annals of Mathematical Statistics*, 22(1):79–86, March 1951.

Jean-Christophe Leloup and Albert Goldbeter. Toward a detailed computational model for the mammalian circadian clock. *PNAS*, 100(12):7051–7056, 2003.

Jean-Christophe Leloup and Albert Goldbeter. Modeling the mammalian circadian clock: Sensitivity analysis and multiplicity of oscillatory mechanisms. *Journal of Theoretical Biology*, 230(4):541–562, October 2004. URL http://www.sciencedirect.com/science/article/B6WMD-4D0Y3RC-1/2/a984153419fbe71b554dbe3059a7bb12.

Joel Levine, Pablo Funes, Harold Dowse, and Jeffrey Hall. Signal analysis of behavioral and molecular cycles. *BMC Neuroscience*, 3(1):1, 2002. ISSN 1471-2202. doi: 10.1186/1471-2202-3-1. URL `http://www.biomedcentral.com/1471-2202/3/1`.

Andrew C. Liu, David K. Welsh, Caroline H. Ko, Hien G. Tran, Eric E. Zhang, Aaron A. Priest, Ethan D. Buhr, Oded Singer, Kirsten Meeker, Inder M. Verma, Francis J. Doyle III, Joseph S. Takahashi, and Steve A. Kay. Intercellular coupling confers robustness against mutations in the scn circadian clock network. *Cell*, 129(3):605–616, May 2007. URL `http://www.sciencedirect.com/science/article/B6WSN-4NMMB5G-R/2/4b4958b5013f5671cbd68a0246cfd69d`.

Stphane Mallat. *A Wavelet Tour of Signal Processing*. Academic Press, 1999.

Martin C. Moore-Ede, Charles A. Czeisler, and Gary S. Richardson. Circadian timekeeping in health and disease. *New England Journal of Medicine*, 309(8):469–476, August 1983. ISSN 0028-4793. URL `http://dx.doi.org/10.1056/NEJM198308253090806`.

D. Morlet, F. Peyrin, P. Desseigne, P. Touboul, and P. Rubel. Time-scale analysis of high-resolution signal-averaged surface ECG using wavelet transformation. In *Proceedings: Computers in Cardiology 1991*, pages 393–396, 1991. doi: {10.1109/CIC.1991.169127}.

Tom S. Price, Julie E. Baggs, Anne M. Curtis, Garret A. FitzGerald, and

John B. Hogenesch. WAVECLOCK: wavelet analysis of circadian oscillation. *Bioinformatics*, 24(23):2794–2795, December 2008. doi: 10.1093/bioinformatics/btn521. URL http://bioinformatics.oxfordjournals.org/cgi/content/abstract/24/23/2794.

Till Roenneberg and David Morse. Two circadian oscillators in one cell. *Nature*, 362(6418):362–364, March 1993. URL http://dx.doi.org/10.1038/362362a0.

Hao Song, Paul Smolen, Evyatar Av-Ron, Douglas A. Baxter, John H. Byrne, Chuck Yeung, Matthew Shtrahman, and Xiao-lun Wu. Stick-and-diffuse and caged diffusion: A comparison of two models of synaptic vesicle dynamics. *Biophys. J.*, 92(10):3407–3424, 2007. URL http://www.biophysj.org/cgi/content/abstract/92/10/3407.

T. L. To, M. A. Henson, E. D. Herzog, and F. J. Doyle. A molecular model for intercellular synchronization in the mammalian circadian clock. *Biophysical Journal*, 92(11):3792–3803, June 2007.

Christopher Torrence and Gilbert P. Compo. A practical guide to wavelet analysis. *Bulletin of the American Meteorological Society*, 79:6178, 1998. URL http://citeseer.ist.psu.edu/article/torrence98practical.html.

Alexis B. Webb, Nikhil Angelo, James E. Huettner, and Erik D. Herzog. Intrinsic, nondeterministic circadian rhythm generation in identi-

fied mammalian neurons. *Proceedings of the National Academy of Sciences*, 106(38):16493–16498, 2009. doi: 10.1073/pnas.0902768106. URL http://www.pnas.org/content/106/38/16493.abstract.

David K. Welsh, Diomedes E. Logothetis, Markus Meister, and Steven M. Reppert. Individual neurons dissociated from rat suprachiasmatic nucleus express independently phased circadian firing rhythms. *Neuron*, 14(4):697–706, April 1995. ISSN 0896-6273. doi: 10.1016/0896-6273(95)90214-7. URL http://www.sciencedirect.com/science/article/B6WSS-4CWYS0K-4/2/77a06789c59285ad6ce04925b470180d.

David K. Welsh, Takato Imaizumi, Steve A. Kay, and Michael W. Young. Real-time reporting of circadian-regulated gene expression by luciferase imaging in plants and mammalian cells. *Methods in Enzymology*, Volume 393:269–288, 2005. URL http://www.sciencedirect.com/science/article/B7CV2-4FWM57C-H/2/7d42e97f065af649402a51d36ee6f074.

David K Welsh, Joseph S Takahashi, and Steve A Kay. Suprachiasmatic nucleus: cell autonomy and network properties. *Annual Review of Physiology*, 72:551–577, March 2010. ISSN 1545-1585. doi: 10.1146/annurev-physiol-021909-135919. URL http://www.ncbi.nlm.nih.gov/pubmed/20148688. PMID: 20148688.

Seung-Hee Yoo, Shin Yamazaki, Phillip L. Lowrey, Kazuhiro Shimomura, Caroline H. Ko, Ethan D. Buhr, Sandra M. Siepka, Hee-Kyung Hong,

Won Jun Oh, Ook Joon Yoo, Michael Menaker, and Joseph S. Takahashi. PERIOD2::LUCIFERASE real-time reporting of circadian dynamics reveals persistent circadian oscillations in mouse peripheral tissues. *Proceedings of the National Academy of Sciences of the United States of America*, 101(15):5339 –5346, April 2004. doi: 10.1073/pnas.0308709101. URL `http://www.pnas.org/content/101/15/5339.abstract`.

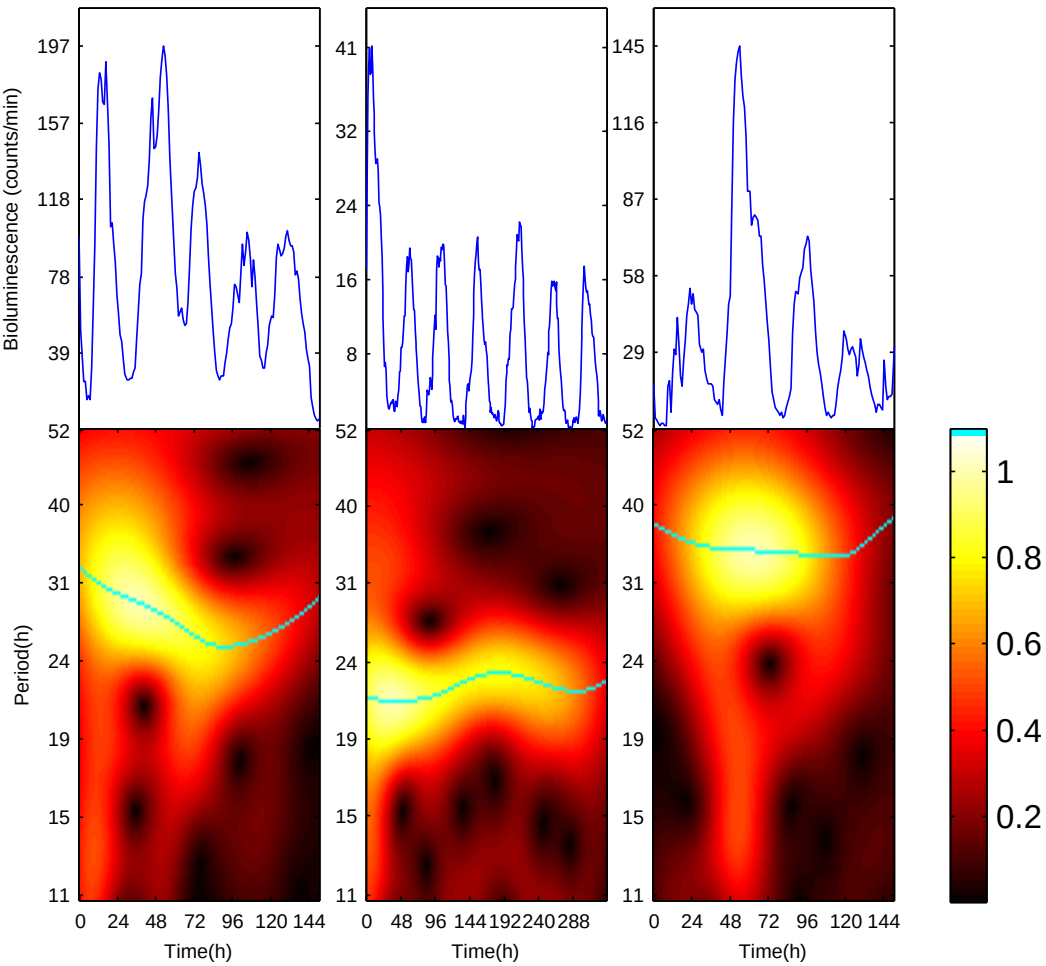

Figure 1: PER2 expression recorded from three representative SCN cells over 7 days showing examples of cells with unstable (A), stable (B), or absent (C) circadian periods. The heatmap plots from each cell show the amplitude of the Continuous Wavelet Transform and the maximum amplitude at each moment (ridge highlighted in green). Note that this ridge plot gradually drifts between 23 and 38 hours in the unstable cell, changes little in the more stable circadian cell, and is consistently infradian (longer than circadian) in the final plot.

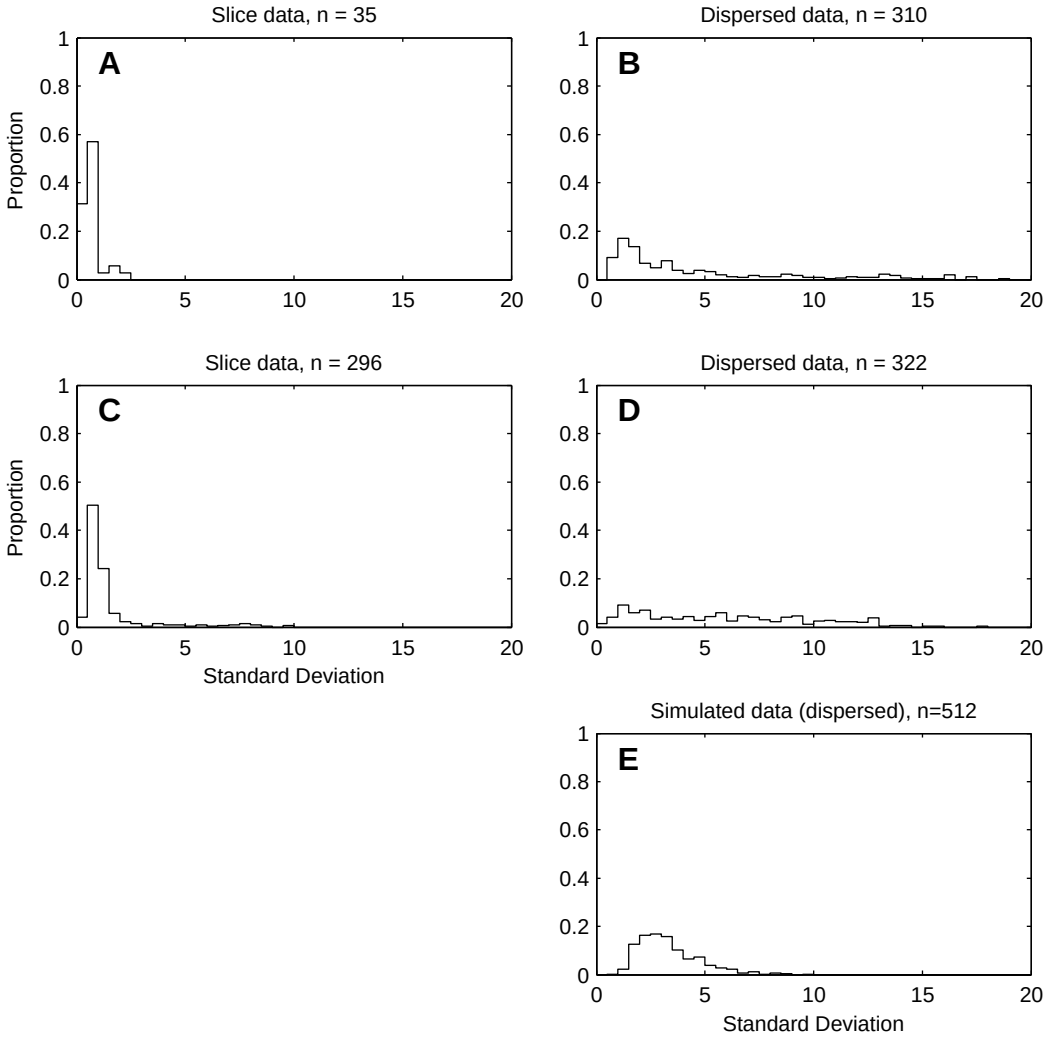

Figure 2: Distribution of the standard deviation of periods across both coupled and dispersed cells from Webb et al., Liu et al., and stochastic modeling. A and B illustrate the distribution of the standard deviation of slice and dispersed cells, respectively, from Liu et al. (2007). C and D illustrate the same statistics for data from Webb et al. (2009). E illustrates the same statistics for dispersed cells in the stochastic model.

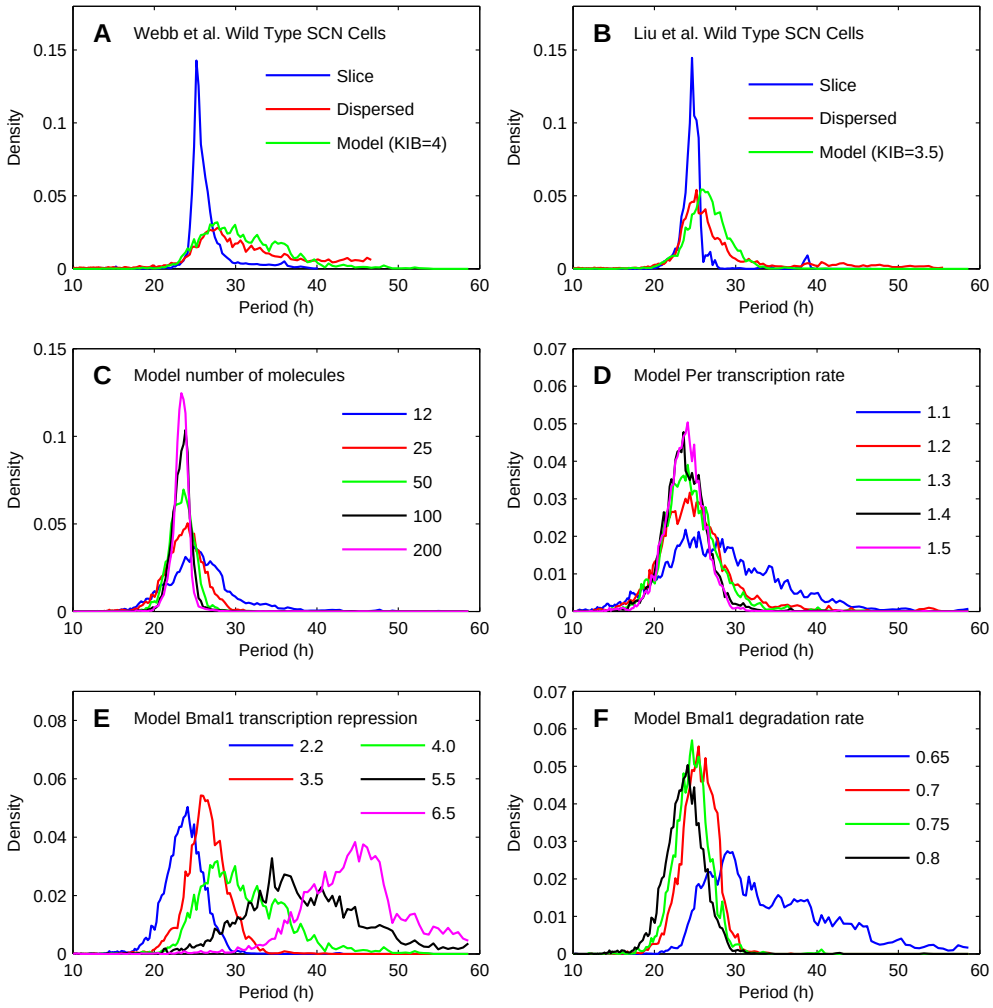

Figure 3: (A-B) The period distributions of dispersed cells from both labs are wider than that of coupled cells (SCN slice) and have a long period tail of up to 48-53 hours. The $K_{IB} = 3.5$ & 4.0 model distributions show the presence of long periods consistent with the biological data. (C) Decreasing the number of molecules in the stochastic model fails to produce the long period tail observed in the biological data. (D) Decreasing the Per transcription rate to very close to the bifurcation point ($\nu_{sP} = 1.1$) begins to produce a long period tail, but the period is less likely to be in the circadian range (24-19 hrs.) than the biological data. (E) Increasing the Bmal1 transcription repression switches the period from the circadian range to long periods (40-50 hrs. for $K_{IB} = 6.5$). (F) Decreasing the Bmal1 degradation rate also produces a switch, but with less probable long periods.

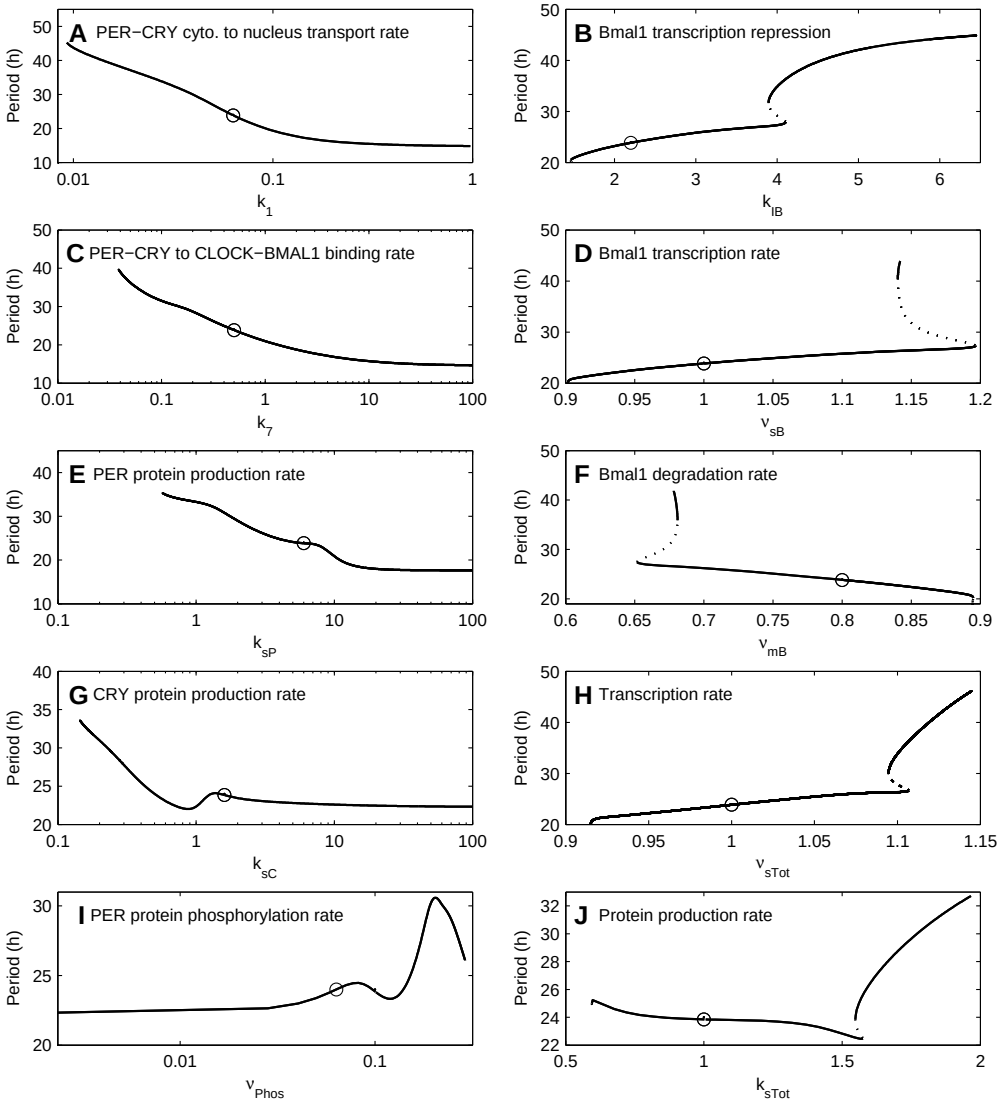

Figure 4: PER-CRY feedback loop parameters (left) and CLOCK-BMAL1 feedback loop parameters and global scale factors (right) that produce long periods. The plots on the left have one stable oscillatory branch and require an order of magnitude change to produce long periods. In contrast, the plots on the right have two stable oscillatory branches (solid line) connected by an unstable oscillatory range (dashed line) and require less than an order of magnitude change to produce long periods. Circles denote the default parameter values.

Table 1: Kullback-Leibler divergence compares period distributions of stochastic model variants with both Webb et al. (2009) and Liu et al. (2007) dispersed wild-type cells. Smaller values of the KL divergence indicate two distributions that are more similar.

Model number of molecules	$\Omega = 12$	$\Omega = 25$	$\Omega = 50$	$\Omega = 100$	$\Omega = 200$
Webb et al. (2009)	**1.56**	10.8	12.3	12.2	17.2
Liu et al. (2007)	**1.29**	4.44	5.47	6.08	8.35
Model Per transcription	$\nu_{sP} = 1.1$	$\nu_{sP} = 1.2$	$\nu_{sP} = 1.3$	$\nu_{sP} = 1.4$	$\nu_{sP} = 1.5$
Webb et al. (2009)	**0.38**	1.66	2.88	4.93	10.8
Liu et al. (2007)	**0.73**	1.32	2.02	2.76	4.44
Model Bmal1 repression	$k_{IB} = 2.2$	$k_{IB} = 3.5$	$k_{IB} = 4.0$	$k_{IB} = 5.5$	$k_{IB} = 6.5$
Webb et al. (2009)	10.8	5.21	**1.34**	1.62	4.74
Liu et al. (2007)	4.44	2.97	**1.48**	2.89	6.19
Model Bmal1 degradation	$\nu_{mB} = 0.65$	$\nu_{mB} = 0.7$	$\nu_{mB} = 0.75$	$\nu_{mB} = 0.8$	
Webb et al. (2009)	**1.88**	10.9	10.0	10.8	
Liu et al. (2007)	**1.86**	4.68	3.83	4.44	